



Arias, L. S., Pessan, J. P., de Souza Neto, F. N., Lima, B. H. R., de Camargo, E. R., Ramage, G., Delbem, A. C. B. and Monteiro, D. R. (2020) Novel nanocarrier of miconazole based on chitosan-coated iron oxide nanoparticles as a nanotherapy to fight Candida biofilms. *Colloids and Surfaces B: Biointerfaces*, 192, 111080. (doi: 10.1016/j.colsurfb.2020.111080)

There may be differences between this version and the published version. You are advised to consult the publisher's version if you wish to cite from it.

<http://eprints.gla.ac.uk/215098/>

Deposited on: 30 April 2020

Enlighten – Research publications by members of the University of Glasgow
<http://eprints.gla.ac.uk>

Novel nanocarrier of miconazole based on chitosan-coated iron oxide nanoparticles as a nanotherapy to fight *Candida* biofilms

Laís Salomão Arias¹, Juliano Pelim Pessan¹, Francisco Nunes de Souza Neto¹, Bruno Henrique Ramos de Lima², Emerson Rodrigues de Camargo³, Gordon Ramage⁴, Alberto Carlos Botazzo Delbem¹, Douglas Roberto Monteiro^{1,5*}

¹São Paulo State University (Unesp), School of Dentistry, Araçatuba, Department of Preventive and Restorative Dentistry, 16015-050 Araçatuba/São Paulo, Brazil;

²nChemi Engenharia de Materiais, 13560-460 São Carlos/São Paulo, Brazil;

³Federal University of São Carlos (UFSCar), Department of Chemistry, 13565-905 São Carlos/São Paulo, Brazil.

⁴Oral Sciences Research Group, Glasgow Dental School, School of Medicine, Dentistry and Nursing, College of Medical, Veterinary and Life Sciences, University of Glasgow, Glasgow, UK, G2 3JZ.

⁵Graduate Program in Dentistry (GPD - Master's Degree), University of Western São Paulo (UNOESTE), 19050-920 Presidente Prudente/São Paulo, Brazil;

***Corresponding author:** Douglas Roberto Monteiro. Graduate Program in Dentistry (GPD - Master's Degree), University of Western São Paulo (UNOESTE). Rua José Bongiovani 700, 19050-920 Presidente Prudente/São Paulo, Brazil. Tel: (+55) 18 3229 1000; E-mail: douglasrmonteiro@hotmail.com

Total number of words: 4553

Figures: 6

Tables: 4

Abstract

Overexposure of microorganisms to conventional drugs has led to resistant species that require new treatment strategies. This study aimed to prepare and characterize a nanocarrier of miconazole (MCZ) based on iron oxide nanoparticles (IONPs) functionalized with chitosan (CS), as well as to test its antifungal activity against biofilms of *Candida albicans* and *Candida glabrata*. IONPs-CS-MCZ nanocarrier was prepared by loading MCZ on CS-covered IONPs and characterized by physicochemical methods. Minimum inhibitory concentration (MIC) of the nanocarrier was determined by the microdilution method. Biofilms were developed (48 h) in microtiter plates and treated with MCZ-carrying nanocarrier at 31.2 and 78 $\mu\text{g/mL}$, in both the presence and absence of an external magnetic field (EMF). Biofilms were evaluated by total biomass, metabolic activity, cultivable cells (CFU), extracellular matrix components, scanning electron microscopy and confocal microscopy. Data were analyzed by two-way ANOVA and Holm-Sidak test ($p < 0.05$). A nanocarrier with diameter lower than 50 nm was obtained, presenting MIC values lower than those found for MCZ, and showing synergism for *C. albicans* and indifference for *C. glabrata*. IONPs-CS-MCZ did not affect total biomass and extracellular matrix. IONPs-CS-MCZ containing 78 $\mu\text{g/mL}$ MCZ showed a superior antibiofilm effect to MCZ in reducing CFU and metabolism for single biofilms of *C. albicans* and dual-species biofilms. The EMF did not improve the nanocarrier effects. Microscopy confirmed the antibiofilm effect of the nanocarrier. IONPs-CS-MCZ was more effective than MCZ mainly against *C. albicans* planktonic cells and number of CFU and metabolism of the biofilms.

Keywords: Biofilms; *Candida*; Chitosan; Ferric oxide; Miconazole; Nanoparticles.

1. Introduction

Candida species are opportunistic yeasts that usually colonize oral cavity, vagina, and respiratory and intestinal tracts of humans [1, 2]. In fact, around 23 to 49% of women over 50 years-old are likely to present vulvovaginal candidiasis [3], while the mortality rate of hospitalized patients with invasive candidiasis ranges from 14 to 80% [4-6]. Moreover, the *Candida* genus is present in the oral microbiome of 25 to 75% of healthy people [7-9]. However, clinical imbalances caused by immunologic shifts, use of dentures, antibiotics and corticosteroids, as well as diabetes, HIV syndrome and other factors can lead to oral candidiasis [7, 10-12]. This clinical condition is characterized by erythematous, pseudomembranous and hyperplastic lesions, and *Candida*-related lesions may also be present, such as angular cheilitis, rhomboid glossitis and denture stomatitis (DS) [7]. *Candida albicans* followed by *Candida glabrata* are frequently detected in cases of oral candidiasis, and are the most prevalent species in DS, an oral disease that affects from 15 to 70% of complete denture wearers [13-15].

Miconazole (MCZ) is an imidazole with topical indication for candidiasis, acting against fungi and a large set of bacteria [16, 17]. Noteworthy, MCZ has shown an antimicrobial effect on fluconazole-resistant *Candida* species [18, 19]. However, MCZ can interact with other drugs, reducing its antimicrobial efficacy, and for some presenting local irritation for some patients [5]. Notably, within biofilms *C. albicans* sessile cells may exhibit tolerance (1 to 10%), even when exposed to high concentrations of MCZ [20]. Moreover, azole cross resistance of *C. albicans* and *C. glabrata* to this antifungal has been reported [21, 22].

The biomedical field has greatly benefited from nanotechnology, as detailed in a comprehensive literature review, with applications for enhancing both the diagnosis and treatment of several diseases [23]. In fact, different pathways (*e.g.*, economic and

ecological routes) have been used for the synthesis of copper, selenium, magnesium oxide and zinc oxide nanoparticles [24-27], which have shown interesting antioxidant and antimicrobial properties.

Among the nanotechnology-based therapies available, drug delivery systems have been developed to increase drug effectiveness and reduce therapeutic concentrations compared to conventional treatments [28]. Recently, nystatin-conjugated bismuth oxide nanoparticles were shown to promote expressive reductions in biofilm formation by *C. albicans* (94.2%) and *Escherichia coli* (84.9%) [29]. Iron oxide magnetic nanoparticles (IONPs) have also been used in different biomedical applications, including drug hyperthermia, magnetic resonance and design of drug delivery systems [30]. Although there are few studies on the antibiofilm activity of IONPs, a recent study showed that the magnetic properties of these nanoparticles may be exploited by using an external magnetic field to conduct IONPs within the biofilm. Here it was reported that by creating artificial channels they have the possibility of enhance drug penetration and thereby increasing the cell death [31].

IONPs surface may be coated with different organic and inorganic compounds (*i.e.* surfactants, polymers, gold, silica, peptides and others), which makes these nanoparticles more biocompatible and prevents their aggregation and oxidation [32]. In this sense, natural polymers such as chitosan (CS) have been used as a nanoparticle coating, owing to the biocompatibility, mucoadhesive, hemostatic and antimicrobial properties of this polymer [32-35]. IONPs-based nanocarriers functionalized with CS proved to be effective against *C. albicans* and different bacteria [36], and successfully favored the efficacy of broad spectrum drugs such as chlorhexidine and fluconazole against oral pathogenic microorganisms *in vitro* [33, 37]. No other work, however, has investigated the use of CS-coated IONPs as a therapeutic tool to improve the antifungal effect of MCZ in order to overcome the above-mentioned limitations of this drug.

Therefore, the aim of this study was to prepare and characterize a MCZ nanocarrier based on CS-coated IONPs, as well as to test its antifungal activity against single- and dual-species biofilms of *C. albicans* and *C. glabrata in vitro*, both in the presence and absence of an external magnetic field. The null hypothesis of the study was that the antifungal effect of the IONP-CS-MCZ nanocarrier would not differ from that observed for MCZ alone, regardless of the presence of an external magnetic field during the treatment period.

2. Materials and methods

2.1. Preparation and characterization of the IONPs-CS-MCZ nanocarrier

Colloidal IONPs (Fe_3O_4) were supplied by *nChemi Engenharia de Materiais* (São Carlos, São Paulo, Brazil), while CS and MCZ were purchased from Sigma-Aldrich (St. Louis, MO, USA). The preparation and characterization of the IONPs-CS-MCZ nanocarrier were conducted as described elsewhere [33]. In brief, CS was solubilized in 2% acetic acid under constant stirring during 24 h at room temperature. CS-coated IONPs were obtained by mixing equal volumes of IONPs and CS, both at 1400 $\mu\text{g/mL}$ of these components. In order to obtain the IONP-CS-MCZ nanocarrier, 500 μg MCZ were added to the IONP-CS compound (700 $\mu\text{g/mL}$), followed by a 1-h solubilization process under constant magnetic stirring at room temperature. Next, the nanocarrier was characterized by transmission electron microscopy (TEM), dynamic light scattering (DLS), X-ray powder diffraction (XRD), Fourier-transform infrared spectroscopy (FTIR) and thermogravimetric analysis (TGA)

2.2. Strains and growth conditions

The present study used two reference strains from American Type Culture Collection (ATCC): *C. albicans* ATCC 10231 and *C. glabrata* ATCC 90030. Stock cultures (-80°C) of both strains were aerobically cultivated on Sabouraud Dextrose Agar (SDA; Difco, Le Pont de Claix, France) plates at 37°C. After 24 h, colonies of both strains from SDA plates were separately inoculated overnight in Sabouraud Dextrose Broth (SDB; Difco) at 37°C. To adjust the inoculum concentration, the fungal cells were harvested by centrifugation (8000 rpm, 5 min) and washed twice in phosphate buffered saline (PBS; pH 7, 0.1 mol/l). Artificial saliva (AS; pH 6.8) [38] was the medium used to resuspend the cells at 1×10^7 cells/mL or 2×10^7 cells/mL, respectively, for single- and dual-species biofilms.

2.3. Determination of the minimum inhibitory concentration (MIC) on planktonic cells

The broth microdilution method was employed to determine the MIC of the IONPs-CS-MCZ nanocarrier against the studied strains, as previously described [39]. Briefly, cell suspensions of *C. albicans* and *C. glabrata* were adjusted in saline solution to a concentration corresponding to the standard 0.5 of McFarland scale (0.5 to 2.5×10^3 cells/mL) and then diluted in saline solution (1:5). Subsequently, this was diluted in Roswell Park Memorial Institute (RPMI 1640; Sigma-Aldrich) medium (1:20). Next, 100 μ L of each yeast suspension were added to the wells of a 96-well flat bottom plate (Costar, Tewksbury, USA) containing 100 μ L of each specific concentration of the nanocarrier (0.09-50 μ g/mL) previously diluted in RPMI 1640. IONPs (0.13-70 μ g/mL), CS (0.13-70 μ g/mL) and MCZ (0.09-50 μ g/mL) alone were tested as controls. After incubation for 48 h at 37°C, the MIC values were visually established as the lowest concentrations capable of completely (100%) inhibiting the yeasts' growth. In order to evaluate the type of interaction among the nanocarrier's compounds, the fractional inhibitory concentration (FIC) indexes were calculated, based on the MIC

results, as detailed elsewhere [40]. MIC assays were repeated in triplicate on three independent occasions.

2.4. Biofilm formation and treatment

For single-species biofilm formation, 200 μL of each yeast suspension (1×10^7 cells/mL in AS) were added into wells of 96-well flat bottom plates, whereas for dual-species biofilms 100 μL of each microbial suspension (2×10^7 cells/mL for *C. albicans* + 2×10^7 cells/mL for *C. glabrata* – [both final conc. of 1×10^7 cells/mL]) were incorporated into each well. The microtiter plates were then aerobically incubated at 37°C. After 48-h biofilm formation (with refreshment of the AS medium after the first 24 h), single- and dual-species biofilms were treated during 24 h with the MCZ-containing nanocarrier at two different concentrations: 31.2 (IONPs-CS-MCZ31.2) and 78 $\mu\text{g/mL}$ (IONPs-CS-MCZ78). These concentrations corresponded to 20- and 50-fold the nanocarrier MIC for *C. glabrata* (1.56 $\mu\text{g/mL}$). All biofilm assays had appropriate controls, including 110 $\mu\text{g/mL}$ IONPs, 110 $\mu\text{g/mL}$ CS, 78 $\mu\text{g/mL}$ MCZ and untreated biofilms as negative control (NC). Biofilm treatment was performed both in the presence and absence of an external magnetic field. For the set of experiments involving magnetic field, magnetic plates (Supergauss Prod. Magnéticos Ltda., São Paulo, Brazil) of $10 \times 100 \times 150$ mm with magnetic flux density between 3900~4000 G were positioned under the 96 well-plates during the 24-h treatment period.

2.5. Biofilm quantification

Following treatment, all biofilms were rinsed once with PBS to remove non-adhered cells, and a crystal violet (CV) staining and XTT reduction assay were employed, respectively, to quantify the total biofilm biomass and metabolic activity of biofilm cells, as previously described [41]. For quantification of colony-forming units

(CFUs) the treated biofilms were scraped from the bottom of the plates, suspended in PBS (1 ml) and homogenized in vortex (90 s). Serial dilutions were then performed in PBS were plated on SDA for single biofilms, and on CHROMagar *Candida* (Difco) for dual-species biofilms. The agar plates were incubated at 37°C, and the CFUs counted after 24 to 48h [40]. The results of total biomass, metabolic activity and number of CFUs were expressed as a function of the well area (Abs/cm² and log₁₀ CFU/cm²).

The compositional analysis of the biofilms' extracellular matrix was also performed. Briefly, single- and dual-species biofilms were developed in 24-well plates containing 1 mL of cell suspension, and treated with the nanocarrier and controls, as detailed above. For matrix extraction, the resulting biofilms were scraped from the wells, resuspended in PBS, sonicated on ice (30 s; 30 w) and vortexed for 2 min. Afterwards, biofilm suspensions were centrifuged at 3000 g for 10 min and the supernatant, filtered through a nitrocellulose filter (0.22 μm) [42, 43]. The protein content of the extracellular matrix was determined by the bicinchoninic acid method (BCA kit; Sigma-Aldrich), using bovine serum albumin as standard [44]. Total carbohydrate content was estimated using glucose as standard [42, 43, 45]. To assess the content of DNA from matrix biofilm, 1.5 μL of the supernatant was pipetted into a NanoDrop device (Eon Microplate Spectrophotometer; Bio Tek, Winooski, USA) and spectrophotometrically analysed at 260 nm and 280 nm [46]. Total contents of protein, carbohydrate and DNA were expressed as a function of the liquid phase of the extracellular matrix (mg/mL).

2.6. Structural analysis of biofilms

Scanning electron microscopy (SEM) and confocal laser scanning microscopy (CLSM) were employed to visualize the ultrastructure of dual-species *Candida* biofilms treated with IONPs-CS-MCZ nanocarrier and controls. For this, biofilms were formed

at the bottom of 24-well plates for SEM, and on sterile coverslips into 24-well plates for CLSM. Biofilm treatment was performed in the absence of an external magnetic field, as described above. For SEM preparation, the samples were serially washed in ethanol for dehydration (70% for 10 min, 95% for 10 min and 100% for 20 min), air-dried in a desiccator, and cut from the bottom of the plates. Samples were then positioned onto aluminum stubs before being coated with gold, and qualitatively analyzed by SEM (FEG-VP Supra 35; Carl Zeiss, Jena, Thüringen, Germany)[39]. As for CLSM analysis, the resulting biofilms were stained with 200 μ L of a solution containing 3 μ g/mL SYTO9 green fluorescent dye and 3 μ g/mL propidium iodide for 20 to 30 min at room temperature, protected from light [42]. Biofilm samples were then gently rinsed with sterile water and analyzed under a confocal microscope (Nikon C2/C2si, Tokyo, Japan) at 488/500-570 nm for SYTO9 dye and 561/570-1000 nm for propidium iodide. Fluorescent green and red colors represent living and dead cells, respectively.

2.7. Statistical analysis

All biofilm assays were conducted in triplicate on three separate occasions. Data presented normal (Shapiro-Wilk test) and homogeneous (Cochrane test) distribution, except for DNA (*C. glabrata* and dual-species biofilms) and protein (*C. albicans* and dual-species biofilms). Results were submitted to 2-way ANOVA, considering the different compounds and the presence of an external magnetic field as variation factors. A Holm-Sidak test was applied for multiple-comparisons when applicable. SigmaPlot software (version 12.0; Systat Software Inc., San Jose, USA) was used, adopting $p < 0.05$ as statistically significant.

3. Results

3.1. Characterization of the IONPs-CS-MCZ nanocarrier

The characterization results of IONPs alone and CS-coated IONPs were previously described by our group [33]. Therefore, this section only presents the characterization of the IONPs-CS-MCZ nanocarrier. TEM and DLS analyzes were used to estimate the morphology and average size of the nanocarrier. By TEM it was possible to observe a predominantly spherical shape for IONPs and MCZ particles, with a diameter lower than 50 nm for the IONPs-CS-MCZ nanocarrier (Fig. 1a). It was also possible to note the MCZ particles adhered to the CS-coated IONPs, thus forming the nanocarrier (Fig. 1a). In turn, DLS analysis showed that the average hydrodynamic size of the nanocarrier was close to 180 nm (Fig. 1b). Regarding the nanocarrier's crystalline structure, the XRD pattern obtained was similar to that seen for IONPs alone, and revealed a spinel-type structure [33].

FTIR analysis revealed the chemical constitution of the IONPs-CS-MCZ nanocarrier. Characteristic bands of IONPs [33] and CS [33] were seen in the nanocarrier's FTIR spectrum (Fig. 1c). Absorption peaks around 1585 cm^{-1} , 1473 cm^{-1} (C-C of two dichlorobenzene), 1385 cm^{-1} (C-C and C-H of imidazole) and 1327 cm^{-1} (C-H of two dichlorobenzene), which are indicative of MCZ [47], were also detected (Fig. 1c). For TGA, a marked mass loss was seen from 200°C , suggesting CS degradation and MCZ melting (Fig. 1d). Analyzing the temperature range from 400 to 800°C , the thermogravimetric curve for IONPs-CS-MCZ (Fig. 1d) showed a similar mass loss pattern to that previously found for IONPs e CS-coated IONPs[33], thus evidencing that all MCZ incorporated was successfully conjugated to the IONPs-CS compound.

3.2. Determination of the MIC

The results of planktonic cell susceptibility testing are shown in Table 1. For *C. albicans*, the nanocarrier promoted an 8-fold reduction in the MCZ MIC value compared to the antifungal applied alone, while for *C. glabrata* this reduction was 2- to 4-fold. Furthermore, *C. albicans* was slightly more susceptible to MCZ and the nanocarrier than *C. glabrata*, whereas IONPs and CS alone did not inhibit the growth of both strains at 140 µg/mL. The association of compounds forming the nanocarrier was then classified as synergistic and indifferent, respectively for *C. albicans* and *C. glabrata*.

3.3. Biofilm quantification

For single- and dual-species biofilms treated in the presence or absence of an external magnetic field, none of the compounds assessed were able to promote significant decreases in total biomass compared to NC groups (Fig. 2).

For *C. albicans* and mixed biofilms, MCZ and IONPs-CS-MCZ78 were shown to be the only compounds that led to significant reductions compared to NCs, both in the presence and in absence of an external magnetic field (Fig. 3a and c). IONPs-CS-MCZ78 significantly differed from all other groups and produced the highest reductions in biofilm metabolism compared to NCs (93.04-94.40%; Fig. 3a and c), regardless of the use of a magnetic field. For single biofilm of *C. glabrata*, MCZ, IONPs-CS-MCZ31.2 and IONPs-CS-MCZ78 did not differ from each other and promoted significant reductions in the metabolic activity (ranging from 64.15 to 98.27%) compared to the NC (Fig. 3b). The use of an external magnetic field did not influence the metabolism results for all biofilms (Fig. 3).

CFU enumeration results for single-species biofilms of *C. albicans* and *C. glabrata* showed that CS, MCZ and IONPs-CS-MCZ31.2 were able to significantly reduce the number of cultivable cells compared to NCs (Fig. 4a and b). However,

IONPs-CS-MCZ78 was the most effective treatment, differing significantly from all groups and promoting cell number decreases in comparison to the NCs ranging from 1.21- to 1.42- \log_{10} in both the presence and absence of an external magnetic field (Fig. 4a and b). For *C. albicans* in dual-species biofilms, IONPS-CS-MCZ78 also exhibited the highest reductions compared to the NCs (1.85-2.05- \log_{10} ; Fig. 4c). As for *C. glabrata* in dual-species biofilms, MCZ and IONPs-CS-MCZ78 were the most effective compounds in reducing the number of CFUs, without significant differences between them (Fig. 4d). The presence of an external magnetic field only influenced the CFU quantification of *C. albicans* in dual-species biofilms treated with IONPs (Fig. 4c).

For all biofilms evaluated, treatments with IONPs-CS-MCZ and controls did not affect protein (Table 2), carbohydrate (Table 3, Supplementary Material) and DNA (Table 4, Supplementary Material) contents of the extracellular matrix. In addition, the use of an external magnetic field during biofilm treatment did not interfere with the results of matrix composition.

3.4. Structural analysis of biofilms

SEM images revealed that the untreated dual-species biofilm consisted of a dense and robust network of interconnected yeasts and hyphae, forming a multilayer structure (Fig. 5a). Biofilms treated with IONPs, CS and IONPs-CS-MCZ31.2 exhibited the same structural pattern observed for the NC group (Fig. 5b, c and e). On the other hand, MCZ and IONPs-CS-MCZ78 produced ruptures in the biofilms, generating less dense structures, with more visualization of polystyrene surface areas (Fig. 5d and f). Some particle agglomerates (CS and IONPs) were also observed in biofilms exposed to CS (Fig. 5c), IONPs-CS-MCZ31.2 (Fig. 5e) and IONPs-CS-MCZ78 (Fig. 5f). According to CLSM images, biofilms treated with CS, MCZ, IONPs-CS-MCZ31.2 and

IONPs-CS-MCZ78 showed higher number of non-viable cells compared to the NC group (Fig. 6).

4. Discussion

The constant exposure of pathogenic microorganisms to conventional drugs has led to improved mechanisms of resistance, making it difficult to treat diseases, thus creating a generation of resistant microorganisms, known as ‘superbugs’ [48]. Within this context, the present study investigated the potential of a nanocarrier based on CS-coated IONPs to improve the antifungal efficacy of MCZ against pathogenic fungal biofilms. The study's null hypothesis was partially rejected, since the nanocarrier effects on planktonic cells and on some biofilm parameters (CFUs for all biofilms, and metabolic activity for single biofilms of *C. albicans* and dual-species biofilms) were superior to those found for MCZ alone.

The results of characterization shown in Fig. 1 evidenced the successful assembly of IONPs-CS-MCZ as a functional nanocarrier. TEM results confirmed a diameter lower than 50 nm for the nanocarrier, which ensures that this conjugate can be explored as an alternative nanotherapy. In contrast, DLS results indicated a large hydrodynamic diameter (around 180 nm; Fig. 1b). DLS is an indirect method that calculates sample size by the frequency of movement of particles in aqueous medium [49]. Thus, this technique is very sensitive to aggregation and may generate different results from those obtained for imaging techniques of dried samples, as TEM [49]. Due to its biocompatibility, biodegradability and stability in acidic pH, CS is frequently used as a coating for IONPs as this polymer usually adsorbs to these nanoparticles through glycosidic bonds [50, 51]. In turn, MCZ probably bound to CS via electrostatic attraction between the amine groups of CS and the negative charge of MCZ [52]. Taken together, these physicochemical phenomena explain how the nanocarrier was formed.

As for MIC determination, IONPs-CS-MCZ was more effective than MCZ alone on *C. albicans* and *C. glabrata* planktonic cells (Table 1). For planktonic *C. albicans*, the nanocarrier effect was the result of a synergistic interaction among the compounds present in the nanocarrier, as shown by the FIC index. MCZ causes accumulation of reactive oxygen species (ROS) in the fungal cytoplasm, which can lead to a fungicidal effect. Moreover, a previous study showed that even before ROS led to cell death, the majority of *C. albicans* cells exposed to MCZ were already necrotic [20]. It was suggested that prior to ROS production, MCZ affects the fungal actin cytoskeleton and creates channels in the mitochondrial membrane [20]. Regarding the mechanisms of antimicrobial action of CS, it was hypothesized that its positive charge interacts with the negatively charged cell membrane phospholipids, leading to increase in the membrane permeability, leakage of cell contents and, consequently, cell death [53]. CS also operates against *C. albicans* antagonizing the SAGA complex, which coordinates Ada2 and ABC transporter-encoding genes such as *CDR1* and *MDR1*, and altering the integrity of cell surface [54]. In addition, IONPs-CS may increase ROS production [55]. All the above-mentioned context could explain the synergistic effect found for IONPs-CS-MCZ on *C. albicans* in planktonic culture, since the nanocarrier combines drugs with different mechanisms of action.

C. glabrata, on the other hand, was shown to be less susceptible to MCZ and nanocarrier, with MIC values 2- to 8-fold higher than those found for *C. albicans* (Table 1). Exposure to MCZ may lead to mitochondrial injuries in *C. glabrata* that cause upregulation of efflux pumps genes (*Cdr1*, *Cdr2*, *Snq2* and *Qndr2*) associated with azole resistance, even before ROS accumulation causes its effect, thus increasing resistance to MCZ for this fungal pathogen [56, 57]. Furthermore, although Ada2 controls antifungal drug tolerance and cell wall integrity in *C. glabrata*, it has a different role from that observed in *C. albicans* and does not regulate ABC transporter-

encoding genes such as *CDR1*, *CDR2* (*PDH1*) or *SNQ2* [58]. Thus, even if CS may attack Ada2 in *C. glabrata*, a different mechanism is involved, which could justify the indifference found for IONPs-CS-MCZ on *C. glabrata* planktonic cells.

Regarding biofilm assays, promising results were found for metabolic activity and CFU counting, considering that the IONPs-CS-MCZ78 nanocarrier was more effective than 78 $\mu\text{g/mL}$ MCZ in reducing these parameters (Figs 3 and 4). These results are in agreement with SEM observations, which demonstrated greater ruptures and ultrastructure alterations in dual-species biofilms promoted by IONPs-CS-MCZ78, compared to other groups (Fig. 5). All treatments also generated biofilms with visually higher presence of dead cells in comparison to NC and IONPs alone, as displayed by CLSM (Fig. 6). As CS and MCZ alone were able to promote significant reductions in CFU and metabolism for some biofilms, the results found for IONPs-CS-MCZ78 may reflect a combined action of the antimicrobial effects of CS and MCZ, as justified for MIC results. The antibiofilm activity of IONPs-CS-MCZ78 was also dependent on the presence of MCZ at 78 $\mu\text{g/mL}$, since a dose-dependent effect was noted in comparison to its counterpart containing 31.2 $\mu\text{g/mL}$ MCZ (IONPs-CS-MCZ31.2). In fact, the simultaneous analysis of SEM and CLSM indicate that despite both nanocarriers (IONPs-CS-MCZ31.2 and IONPs-CS-MCZ78) led to higher proportions of non-viable cells compared with the NC group, only the nanocarrier at the highest concentration (IONPs-CS-MCZ78) promoted marked ruptures within the biofilms (Fig. 5 and 6). On the other hand, nanocarrier and controls did not affect the total biofilm biomass (Fig. 2) and extracellular matrix components (Tables 2, 3 and 4). Therefore, all biofilm results analyzed together indicate that the IONPs-CS-MCZ78 nanocarrier was able to cross the extracellular matrix without changing it, exclusively by acting at cellular level (affecting cell viability and metabolism). Indeed, nanocarriers are built for the purpose of

circumventing the physical barriers and penetrating at the most profound layers of the biofilm, due to its size advantages [32].

Magnetic nanoparticles may be additionally guided by external magnetic forces to the cell target [59]. Inside biofilms, magnetic fields may create artificial channels and increase drug penetration, improving the antimicrobial effect [31, 60]. In this sense, the current study tested whether the presence of a static one-side magnetic field (positioned at the bottom of 96-well plates) would add any benefit to the nanocarrier's antibiofilm effect. However, in general the quantitative results showed no differences between biofilms treated in both the presence and absence of an external magnetic field. It is highly likely that the prolonged time of treatment used (24 h) might have been sufficient for nanocarrier penetration into the deeper layers of biofilms treated in the absence of magnetic field, so that any possible effect occurring within the initial exposure time could not be observed. Furthermore, this study did not use a switched magnetic field, which could create additional channels and improve drug efficacy [61].

Another interesting result was the higher effectiveness of the IONPs-CS-MCZ78 nanocarrier compared to MCZ alone, mainly for *C. albicans* in single- and dual-species biofilms (Figs 3 and 4). From a clinical perspective, these findings highlight the potential of the MCZ nanocarrier as a topical treatment to fight recurrent oral candidiasis in which *C. albicans* plays a major role, such as DS. However, to broaden the knowledge about this nanocarrier, future studies assessing the MCZ release profiles, different treatment periods, as well as toxicity to human cells caused by IONPs-CS-MCZ are needed.

5. Conclusion

The protocol used in the present study was successful for the assembly of the IONPs-CS-MCZ nanocarrier, revealing a spinel-structure (IONPs) enveloped by CS and

MCZ, with size smaller than 50 nm. The resulting nanocarrier showed superior antifungal effect to MCZ alone on planktonic cells of *C. albicans* (synergistic effect), while for *C. glabrata* cells an indifferent effect was observed. For biofilm assays, the nanocarrier containing 78 µg/mL MCZ led to higher reductions in some parameters of single- and dual-species biofilms (cultivable cells and metabolism) compared with free MCZ. Additionally, the nanocarrier advantage was more evident for *C. albicans*, suggesting a potential application for the treatment of oral candidiasis in which this fungus is the main responsible. The presence of an external magnetic field during biofilm treatment did not potentiate the nanocarrier's antibiofilm effect.

Acknowledgements

The authors thank *nChemi Engenharia de Materiais* for supplying the iron oxide nanoparticles, and LabMicro – FCT/Unesp (School of Technology and Applied Sciences (FCT), São Paulo State University (Unesp), Presidente Prudente/São Paulo, Brazil), especially Mr. José Diego Fernandes and Prof. Carlos José Leopoldo Constantino for obtaining the confocal fluorescence images.

Funding sources

This study was supported by the São Paulo Research Foundation (FAPESP, Grant# 2017/24416-2), Conselho Nacional de Desenvolvimento Científico e Tecnológico (CNPq, Brazil; scholarship to the first author and Grant# 404721/2016-8) and the Coordenação de Aperfeiçoamento de Pessoal de Nível Superior (CAPES, Finance Code 001).

Conflict of Interest

The authors declare no conflict of interest.

Authors' Contributions

L.S.A. participated in the study design, performed all microbiological tests, collaborated with the nanocarrier characterization assays and analysis of biofilm structure, and wrote the manuscript. F.N.S.N. and B.H.R.L. collaborated with the assembly and characterization of the nanocarrier, and revised the article. J.P.P., E.R.C., G.R. and A.C.B.D. analyzed the data and critically reviewed the article. DRM conceived the study, analyzed the data, and revised the final version of the manuscript. All authors have read and approved the final manuscript.

References

- [1] N.N. Mishra, T. Prasad, N. Sharma, A. Payasi, R. Prasad, D.K. Gupta, R. Singh, Pathogenicity and drug resistance in *Candida albicans* and other yeast species. A review, *Acta Microbiol Immunol Hung*, 54 (2007) 201-235.
- [2] D.L. Moyes, J.R. Naglik, Mucosal immunity and *Candida albicans* infection, *Clin Dev Immunol*, 2011 (2011) 346307.
- [3] F. Blostein, E. Levin-Sparenberg, J. Wagner, B. Foxman, Recurrent vulvovaginal candidiasis, *Ann Epidemiol*, 27 (2017) 575-582 e573.
- [4] L.L. Castro, M. Schutze, D.H. Bucker, S. Vasconcellos Lde, Prevalence of fungemia in a tertiary hospital: Analysis of the last decade, *Rev Assoc Med Bras* (1992), 62 (2016) 315-319.
- [5] L.S. Rodrigues, F.A. Motta, G.L. Picharski, T.M. Vasconcelos, M.C. Ricciari, L.M. Dalla-Costa, Invasive candidiasis: Risk factor for mortality in a pediatric tertiary care hospital in south of Brazil, *Medicine (Baltimore)*, 98 (2019) e15933.
- [6] J.A. Cortes, P. Reyes, C.H. Gomez, S.I. Cuervo, P. Rivas, C.A. Casas, R. Sanchez, Clinical and epidemiological characteristics and risk factors for mortality in patients

with candidemia in hospitals from Bogota, Colombia, *Braz J Infect Dis*, 18 (2014) 631-637.

[7] G. Quindos, S. Gil-Alonso, C. Marcos-Arias, E. Sevillano, E. Mateo, N. Jauregizar, E. Eraso, Therapeutic tools for oral candidiasis: Current and new antifungal drugs, *Med Oral Patol Oral Cir Bucal*, 24 (2019) e172-e180.

[8] K. Zomorodian, N.N. Haghghi, N. Rajaei, K. Pakshir, B. Tarazooie, M. Vojdani, F. Sedaghat, M. Vosoghi, Assessment of *Candida* species colonization and denture-related stomatitis in complete denture wearers, *Med Mycol*, 49 (2011) 208-211.

[9] N.S. Dar-Odeh, A.A. Shehabi, Oral candidosis in patients with removable dentures, *Mycoses*, 46 (2003) 187-191.

[10] L.A. Gaitan-Cepeda, O. Sanchez-Vargas, N. Castillo, Prevalence of oral candidiasis in HIV/AIDS children in highly active antiretroviral therapy era. A literature analysis, *Int J STD AIDS*, 26 (2015) 625-632.

[11] F. Javed, A.A. Al-Kheraif, S.V. Kellesarian, F. Vohra, G.E. Romanos, Oral *Candida* carriage and species prevalence in denture stomatitis patients with and without diabetes, *J Biol Regul Homeost Agents*, 31 (2017) 343-346.

[12] K. Zomorodian, F. Kavooosi, G.R. Pishdad, P. Mehriar, H. Ebrahimi, A. Bandegani, K. Pakshir, Prevalence of oral *Candida* colonization in patients with diabetes mellitus, *J Mycol Med*, 26 (2016) 103-110.

[13] Q. Li, J. Liu, J. Shao, W. Da, G. Shi, T. Wang, D. Wu, C. Wang, Decreasing Cell Population of Individual *Candida* Species Does Not Impair the Virulence of *Candida albicans* and *Candida glabrata* Mixed Biofilms, *Front Microbiol*, 10 (2019) 1600.

[14] L. Gendreau, Z.G. Loewy, Epidemiology and etiology of denture stomatitis, *J Prosthodont*, 20 (2011) 251-260.

- [15] S. Mahdavi Omran, M. Rezaei Dastjerdi, M. Zuashkiani, V. Moqarabzadeh, M. Taghizadeh-Armaki, In Vitro Antifungal Susceptibility of Candida Species Isolated from Iranian Patients with Denture Stomatitis, *Biomed Res Int*, 2018 (2018) 3086586.
- [16] N. Delattin, B.P. Cammue, K. Thevissen, Reactive oxygen species-inducing antifungal agents and their activity against fungal biofilms, *Future Med Chem*, 6 (2014) 77-90.
- [17] L.W. Zhang, J.Y. Fu, H. Hua, Z.M. Yan, Efficacy and safety of miconazole for oral candidiasis: a systematic review and meta-analysis, *Oral Dis*, 22 (2016) 185-195.
- [18] N. Isham, M.A. Ghannoum, Antifungal activity of miconazole against recent Candida strains, *Mycoses*, 53 (2010) 434-437.
- [19] J.A. Vazquez, J.D. Sobel, Miconazole mucoadhesive tablets: a novel delivery system, *Clin Infect Dis*, 54 (2012) 1480-1484.
- [20] D. Vandenbosch, K. Braeckmans, H.J. Nelis, T. Coenye, Fungicidal activity of miconazole against Candida spp. biofilms, *J Antimicrob Chemother*, 65 (2010) 694-700.
- [21] E.W. Cross, S. Park, D.S. Perlin, Cross-Resistance of clinical isolates of Candida albicans and Candida glabrata to over-the-counter azoles used in the treatment of vaginitis, *Microb Drug Resist*, 6 (2000) 155-161.
- [22] K. Miranda-Cadena, C. Marcos-Arias, E. Mateo, J.M. Aguirre, G. Quindos, E. Eraso, Prevalence and antifungal susceptibility profiles of Candida glabrata, Candida parapsilosis and their close-related species in oral candidiasis, *Arch Oral Biol*, 95 (2018) 100-107.
- [23] M. Abd Elkodous, G.S. El-Sayyad, I.Y. Abdelrahman, H.S. El-Bastawisy, A.E. Mohamed, F.M. Mosallam, H.A. Nasser, M. Gobara, A. Baraka, M.A. Elsayed, A.I. El-Batal, Therapeutic and diagnostic potential of nanomaterials for enhanced biomedical applications, *Colloids Surf B Biointerfaces*, 180 (2019) 411-428.

- [24] A.I. El-Batal, N.E. Al-Hazmi, F.M. Mosallam, G.S. El-Sayyad, Biogenic synthesis of copper nanoparticles by natural polysaccharides and *Pleurotus ostreatus* fermented fenugreek using gamma rays with antioxidant and antimicrobial potential towards some wound pathogens, *Microb Pathog*, 118 (2018) 159-169.
- [25] F.M. Mosallam, G.S. El-Sayyad, R.M. Fathy, A.I. El-Batal, Biomolecules-mediated synthesis of selenium nanoparticles using *Aspergillus oryzae* fermented Lupin extract and gamma radiation for hindering the growth of some multidrug-resistant bacteria and pathogenic fungi, *Microb Pathog*, 122 (2018) 108-116.
- [26] G.S. El-Sayyad, F.M. Mosallam, A.I. El-Batal, One-pot green synthesis of magnesium oxide nanoparticles using *Penicillium chrysogenum* melanin pigment and gamma rays with antimicrobial activity against multidrug-resistant microbes, *Advanced Powder Technology*, 29 (2018) 2616-2625.
- [27] M. Abd Elkodous, G.S. El-Sayyad, M.I.A. Abdel Maksoud, I.Y. Abdelrahman, F.M. Mosallam, M. Gobara, A.I. El-Batal, Fabrication of Ultra-Pure Anisotropic Zinc Oxide Nanoparticles via Simple and Cost-Effective Route: Implications for UTI and EAC Medications, *Biol Trace Elem Res*, (2019).
- [28] Y.H. Yun, B.K. Lee, K. Park, Controlled Drug Delivery: Historical perspective for the next generation, *J Control Release*, 219 (2015) 2-7.
- [29] A.I. El-Batal, H.G. Nada, R.R. El-Behery, M. Gobara, G.S. El-Sayyad, Nystatin-mediated bismuth oxide nano-drug synthesis using gamma rays for increasing the antimicrobial and antibiofilm activities against some pathogenic bacteria and *Candida* species, *RSC Advances*, 10 (2020) 9274-9289.
- [30] G.R. Rodrigues, C. Lopez-Abarrategui, I. de la Serna Gomez, S.C. Dias, A.J. Otero-Gonzalez, O.L. Franco, Antimicrobial magnetic nanoparticles based-therapies for controlling infectious diseases, *Int J Pharm*, 555 (2019) 356-367.

- [31] K. Quan, Z. Zhang, H. Chen, X. Ren, Y. Ren, B.W. Peterson, H.C. van der Mei, H.J. Busscher, Artificial Channels in an Infectious Biofilm Created by Magnetic Nanoparticles Enhanced Bacterial Killing by Antibiotics, *Small*, 15 (2019) e1902313.
- [32] L.S. Arias, J.P. Pessan, A.P.M. Vieira, T.M.T. Lima, A.C.B. Delbem, D.R. Monteiro, Iron Oxide Nanoparticles for Biomedical Applications: A Perspective on Synthesis, Drugs, Antimicrobial Activity, and Toxicity, *Antibiotics (Basel)*, 7 (2018).
- [33] A.P.M. Vieira, L.S. Arias, F.N. de Souza Neto, A.M. Kubo, B.H.R. Lima, E.R. de Camargo, J.P. Pessan, A.C.B. Delbem, D.R. Monteiro, Antibiofilm effect of chlorhexidine-carrier nanosystem based on iron oxide magnetic nanoparticles and chitosan, *Colloids Surf B Biointerfaces*, 174 (2019) 224-231.
- [34] J.H. Juang, C.R. Shen, J.J. Wang, C.H. Kuo, Y.W. Chien, H.Y. Kuo, F.R. Chen, M.H. Chen, T.C. Yen, Z.T. Tsai, Magnetic resonance imaging of mouse islet grafts labeled with novel chitosan-coated superparamagnetic iron oxide nanoparticles, *PLoS One*, 8 (2013) e62626.
- [35] P.I. Soares, D. Machado, C. Laia, L.C. Pereira, J.T. Coutinho, I.M. Ferreira, C.M. Novo, J.P. Borges, Thermal and magnetic properties of chitosan-iron oxide nanoparticles, *Carbohydr Polym*, 149 (2016) 382-390.
- [36] P. Nehra, R.P. Chauhan, N. Garg, K. Verma, Antibacterial and antifungal activity of chitosan coated iron oxide nanoparticles, *Br J Biomed Sci*, 75 (2018) 13-18.
- [37] T.M. de Lima, L.S. Arias, L.F. Afanaci, R.F. Ferraresse, S.N.F.N. de, B.H. de Lima, F.G. Straioto, E.R. de Camargo, J.P. Pessan, D.R. Monteiro, Assembly and antifungal effect of a new fluconazole-carrier nanosystem, *Future Microbiol*, 15 (2020) 273-285.
- [38] H. Lamfon, S.R. Porter, M. McCullough, J. Pratten, Formation of *Candida albicans* biofilms on non-shedding oral surfaces, *Eur J Oral Sci*, 111 (2003) 465-471.

- [39] L.S. Arias, A.C. Delbem, R.A. Fernandes, D.B. Barbosa, D.R. Monteiro, Activity of tyrosol against single and mixed-species oral biofilms, *J Appl Microbiol*, 120 (2016) 1240-1249.
- [40] L.R. do Vale, A. Delbem, L.S. Arias, R.A. Fernandes, A. Vieira, D.B. Barbosa, D.R. Monteiro, Differential effects of the combination of tyrosol with chlorhexidine gluconate on oral biofilms, *Oral Dis*, 23 (2017) 537-541.
- [41] R.A. Fernandes, D.R. Monteiro, L.S. Arias, G.L. Fernandes, A.C. Delbem, D.B. Barbosa, Biofilm formation by *Candida albicans* and *Streptococcus mutans* in the presence of farnesol: a quantitative evaluation, *Biofouling*, 32 (2016) 329-338.
- [42] R.A. Fernandes, D.R. Monteiro, L.S. Arias, G.L. Fernandes, A.C.B. Delbem, D.B. Barbosa, Virulence Factors in *Candida albicans* and *Streptococcus mutans* Biofilms Mediated by Farnesol, *Indian J Microbiol*, 58 (2018) 138-145.
- [43] S. Silva, M. Henriques, A. Martins, R. Oliveira, D. Williams, J. Azeredo, Biofilms of non-*Candida albicans* *Candida* species: quantification, structure and matrix composition, *Med Mycol*, 47 (2009) 681-689.
- [44] D.R. Monteiro, L.S. Arias, R.A. Fernandes, F.G. Straioto, D. Barros Barbosa, J.P. Pessan, A.C.B. Delbem, Role of tyrosol on *Candida albicans*, *Candida glabrata* and *Streptococcus mutans* biofilms developed on different surfaces, *Am J Dent*, 30 (2017) 35-39.
- [45] M. Dubois, K. Gilles, J.K. Hamilton, P.A. Rebers, F. Smith, A colorimetric method for the determination of sugars, *Nature*, 168 (1951) 167.
- [46] T.P. Cavazana, T.Y. Hosida, J.P. Pessan, C. Sampaio, D.R. Monteiro, A.C.B. Delbem, Activity of sodium trimetaphosphate, associated or not with fluoride, on dual-species biofilms, *Biofouling*, (2019) 1-9.
- [47] V. Barillaro, G. Dive, E. Ziemons, P. Bertholet, B. Evrard, L. Delattre, G. Piel, Theoretical and experimental vibrational study of miconazole and its dimers with

organic acids: application to the IR characterization of its inclusion complexes with cyclodextrins, *Int J Pharm*, 350 (2008) 155-165.

[48] M. Honigsbaum, Superbugs and us, *The Lancet*, 391 (2018).

[49] I. Khmara, O. Strbak, V. Zavisova, M. Koneracka, M. Kubovcikova, I. Antal, V. Kavecansky, D. Lucanska, D. Dobrota, P. Kopcansky, Chitosan-stabilized iron oxide nanoparticles for magnetic resonance imaging, *Journal of Magnetism and Magnetic Materials*, 474 (2019) 319-325.

[50] A. López-Cruz, C. Barrera, V.L. Calero-DdelC, C. Rinaldi, Water dispersible iron oxide nanoparticles coated with covalently linked chitosan, *Journal of Materials Chemistry*, 19 (2009).

[51] S.H. Hussein-Al-Ali, M.E. El Zowalaty, M.Z. Hussein, M. Ismail, T.J. Webster, Synthesis, characterization, controlled release, and antibacterial studies of a novel streptomycin chitosan magnetic nanoantibiotic, *Int J Nanomedicine*, 9 (2014) 549-557.

[52] A. Fernandes Costa, D. Evangelista Araujo, M. Santos Cabral, I. Teles Brito, L. Borges de Menezes Leite, M. Pereira, A. Correa Amaral, Development, characterization, and in vitro-in vivo evaluation of polymeric nanoparticles containing miconazole and farnesol for treatment of vulvovaginal candidiasis, *Med Mycol*, 57 (2019) 52-62.

[53] L.Y. Ing, N.M. Zin, A. Sarwar, H. Katas, Antifungal activity of chitosan nanoparticles and correlation with their physical properties, *Int J Biomater*, 2012 (2012) 632698.

[54] P.Y. Shih, Y.T. Liao, Y.K. Tseng, F.S. Deng, C.H. Lin, A Potential Antifungal Effect of Chitosan Against *Candida albicans* Is Mediated via the Inhibition of SAGA Complex Component Expression and the Subsequent Alteration of Cell Surface Integrity, *Front Microbiol*, 10 (2019) 602.

- [55] M. Arakha, S. Pal, D. Samantarrai, T.K. Panigrahi, B.C. Mallick, K. Pramanik, B. Mallick, S. Jha, Antimicrobial activity of iron oxide nanoparticle upon modulation of nanoparticle-bacteria interface, *Scientific Reports*, 5 (2015) 14813.
- [56] D. Sanglard, F. Ischer, J. Bille, Role of ATP-binding-cassette transporter genes in high-frequency acquisition of resistance to azole antifungals in *Candida glabrata*, *Antimicrob Agents Chemother*, 45 (2001) 1174-1183.
- [57] A. Defontaine, J.P. Bouchara, P. Declerk, C. Planchenault, D. Chabasse, J.N. Hallet, In-vitro resistance to azoles associated with mitochondrial DNA deficiency in *Candida glabrata*, *J Med Microbiol*, 48 (1999) 663-670.
- [58] S.J. Yu, Y.L. Chang, Y.L. Chen, Deletion of ADA2 Increases Antifungal Drug Susceptibility and Virulence in *Candida glabrata*, *Antimicrob Agents Chemother*, 62 (2018).
- [59] M. Arruebo, R. Fernández-Pacheco, M.R. Ibarra, J. Santamaría, Magnetic nanoparticles for drug delivery, *Nano Today*, 2 (2007) 22-32.
- [60] J. Li, R. Nickel, J. Wu, F. Lin, J. van Lierop, S. Liu, A new tool to attack biofilms: driving magnetic iron-oxide nanoparticles to disrupt the matrix, *Nanoscale*, 11 (2019) 6905-6915.
- [61] M. Osiński, W.J. Parak, X.-J. Liang, G. Alas, R.E. Pagano, J.Q. Nguyen, H.M.H.N. Bandara, S.A. Ivanov, G.A. Smolyakov, D.L. Huber, H.D.C. Smyth, M. Osiński, Effects of iron-oxide nanoparticles and magnetic fields on oral biofilms, *Colloidal Nanoparticles for Biomedical Applications XII*, 2017.

Table and figure captions

Table 1. Minimum inhibitory concentration (MIC) values of iron oxide magnetic nanoparticles (IONPs), chitosan (CS) and miconazole (MCZ), alone or in association, for the tested *Candida* strains

Table 2. Mean values (standard deviation) of the protein content obtained from the extracellular matrix of single- and dual-species *Candida* biofilms after treatment with different compounds

Figure 1. Transmission electron microscopy image (a), size distribution histogram (b), Fourier-transform infrared spectrum (c) and thermogravimetric analysis (d) for the iron oxide magnetic nanoparticles-chitosan-miconazole nanocarrier. Enlarged image in (a) represents the core of a chitosan-coated nanoparticle, and miconazole particles bound to chitosan. Red circle in (c) shows the region of characteristic bands of the presence of miconazole.

Figure 2. Quantification of total biomass (mean absorbance values per cm^2) for single- (a and b) and dual-species (c) biofilms of *C. albicans* ATCC 10231 and *C. glabrata* ATCC 90030 treated with 110 $\mu\text{g}/\text{mL}$ iron oxide magnetic nanoparticles (IONPs), 110

$\mu\text{g/mL}$ chitosan (CS), $78 \mu\text{g/mL}$ miconazole (MCZ) and MCZ-containing nanocarrier at 31.2 (IONPs-CS-MCZ31.2) and $78 \mu\text{g/mL}$ (IONPs-CS-MCZ78), in the absence or presence of an external magnetic field. Negative control denotes non-treated biofilms (NC). Different uppercase and lowercase letters show significant differences among the treatments for biofilms treated in the absence and presence of an external magnetic field, respectively (2-way ANOVA and Holm-Sidak test, $p < 0.05$).

Figure 3. Quantification of metabolic activity (mean absorbance values per cm^2) for single- (a and b) and dual-species (c) biofilms of *C. albicans* ATCC 10231 and *C. glabrata* ATCC 90030 treated with $110 \mu\text{g/mL}$ iron oxide magnetic nanoparticles (IONPs), $110 \mu\text{g/mL}$ chitosan (CS), $78 \mu\text{g/mL}$ miconazole (MCZ) and MCZ-containing nanocarrier at 31.2 (IONPs-CS-MCZ31.2) and $78 \mu\text{g/mL}$ (IONPs-CS-MCZ78), in the absence or presence of an external magnetic field. Negative control denotes non-treated biofilms (NC). Different uppercase and lowercase letters show significant differences among the treatments for biofilms treated in the absence and presence of an external magnetic field, respectively (2-way ANOVA and Holm-Sidak test, $p < 0.05$).

Figure 4. Quantification of cultivable cells (mean values of the logarithm of colony-forming units per cm^2) for single- (a and b) and dual-species (c and d) biofilms of *C. albicans* ATCC 10231 and *C. glabrata* ATCC 90030 treated with $110 \mu\text{g/mL}$ iron oxide magnetic nanoparticles (IONPs), $110 \mu\text{g/mL}$ chitosan (CS), $78 \mu\text{g/mL}$ miconazole (MCZ) and MCZ-containing nanocarrier at 31.2 (IONPs-CS-MCZ31.2) and $78 \mu\text{g/mL}$ (IONPs-CS-MCZ78), in the absence or presence of an external magnetic field. Negative control denotes non-treated biofilms (NC). Different uppercase and lowercase letters show significant differences among the treatments for biofilms treated in the absence and presence of an external magnetic field, respectively (2-way ANOVA and Holm-

Sidak test, $p < 0.05$). Within each treatment, asterisk (*) indicates significant difference between biofilms treated in the absence and presence of an external magnetic field.

Figure 5. Scanning electron microscopy images of dual-species biofilms of *Candida albicans* ATCC 10231 and *C. glabrata* ATCC 90030 treated with 110 $\mu\text{g/mL}$ iron oxide magnetic nanoparticles (b), 110 $\mu\text{g/mL}$ chitosan (c), 78 $\mu\text{g/mL}$ miconazole (d) and miconazole-containing nanocarrier at 31.2 (e) and 78 $\mu\text{g/mL}$ (f). Negative control denotes non-treated biofilm (a). Magnification: 2500x. Bars: 10 μm . Red arrows in images (c), (e) and (f) indicate particle clusters.

Figure 6. Confocal laser scanning microscopy images of dual-species biofilms of *Candida albicans* ATCC 10231 and *C. glabrata* ATCC 90030 treated with 110 $\mu\text{g/mL}$ iron oxide magnetic nanoparticles (b), 110 $\mu\text{g/mL}$ chitosan (c), 78 $\mu\text{g/mL}$ miconazole (d) and miconazole-containing nanocarrier at 31.2 (e) and 78 $\mu\text{g/mL}$ (f). Negative control denotes non-treated biofilm (a). Magnification: 20x. Bars: 100 μm .

Table 1. Minimum inhibitory concentration (MIC) values of iron oxide magnetic nanoparticles (IONPs), chitosan (CS) and miconazole (MCZ), alone or in association, for the tested *Candida* strains

Species	MIC ($\mu\text{g/ml}$)						FICI	Classification
	Alone			In association (Nanocarrier)				
	IONPs	CS	MCZ	IONPs	CS	MCZ		
<i>C. albicans</i> ATCC 10231	> 140	> 140	1.56	0.27	0.27	0.19	< 0.12	Synergism
<i>C. glabrata</i> ATCC 90030	> 140	> 140	3.12– 6.25	2.18	2.18	1.56	< 0.53	Indifference

Note: FICI, fractional inhibitory concentration indices for the nanocarrier

Table 2. Mean values (standard deviation) of the protein content obtained from the extracellular matrix of single- and dual-species *Candida* biofilms after treatment with different compounds

Biofilms	Proteins (mg/ml)					
	NC	IONPs	CS	MCZ	IONPs-CS-MCZ31.2	IONPs-CS-MCZ78
Presence of an external magnetic field						
<i>C. albicans ATCC 10231</i>	0.10 (0.05)	0.09 (0.00)	0.08 (0.01)	0.09 (0.02)	0.11 (0.03)	0.07 (0.02)
<i>C. glabrata ATCC 90030</i>	0.04 (0.01)	0.07 (0.01)	0.08 (0.02)	0.04 (0.00)	0.06 (0.01)	0.06 (0.03)
<i>Dual-species biofilm</i>	0.12 (0.09)	0.09 (0.04)	0.11 (0.04)	0.09 (0.05)	0.11 (0.02)	0.08 (0.00)
Absence of an external magnetic field						
<i>C. albicans ATCC 10231</i>	0.09 (0.02)	0.12 (0.08)	0.12 (0.06)	0.11 (0.05)	0.13 (0.05)	0.08 (0.01)
<i>C. glabrata ATCC 90030</i>	0.06 (0.03)	0.10 (0.04)	0.09 (0.04)	0.05 (0.01)	0.06 (0.03)	0.05 (0.00)
<i>Dual-species biofilm</i>	0.12 (0.08)	0.06 (0.03)	0.07 (0.02)	0.05 (0.01)	0.08 (0.04)	0.09 (0.06)

Note: there were no statistically significant differences among the compounds, regardless of the presence of a magnetic field (2-way ANOVA; $p < 0.05$). Negative control (NC); 110 $\mu\text{g/ml}$ iron oxide magnetic nanoparticles (IONPs); 110 $\mu\text{g/ml}$ chitosan (CS); 78 $\mu\text{g/ml}$ miconazole (MCZ); MCZ-containing nanocarrier at 31.2 (IONPs-CS-MCZ31.2) and 78 $\mu\text{g/ml}$ (IONPs-CS-MCZ78).

Table 3. Mean values (standard deviation) of the carbohydrate content obtained from the extracellular matrix of single- and dual-species *Candida* biofilms after treatment with different compounds

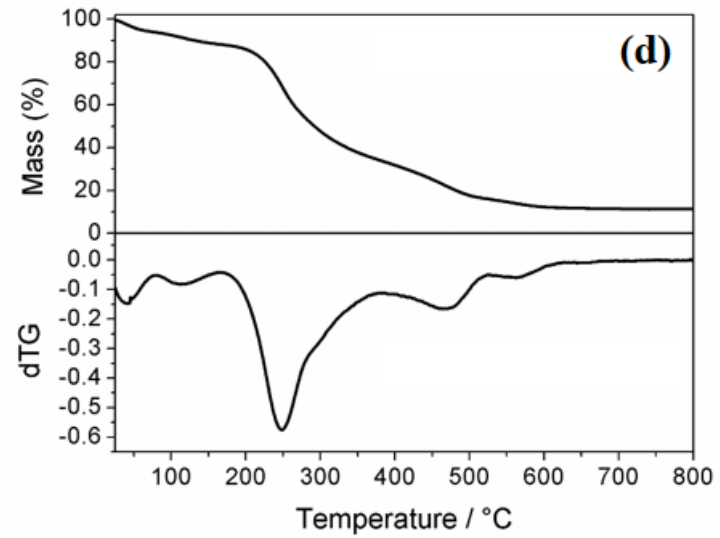
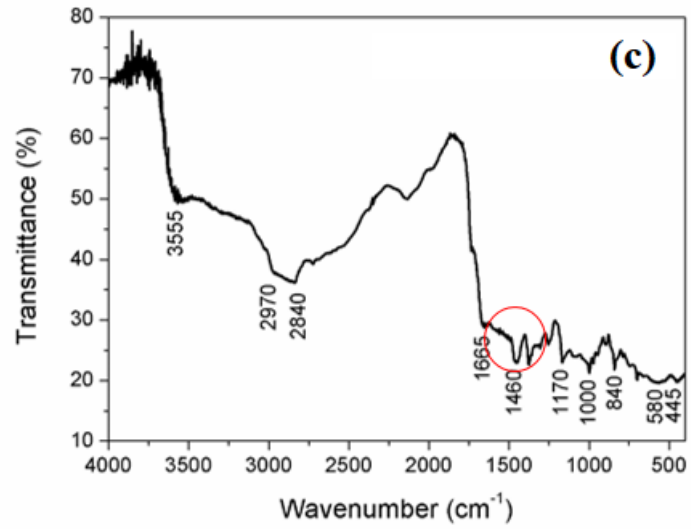
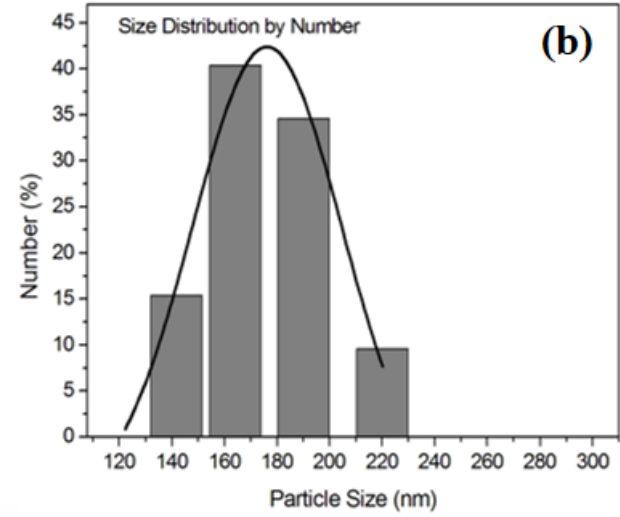
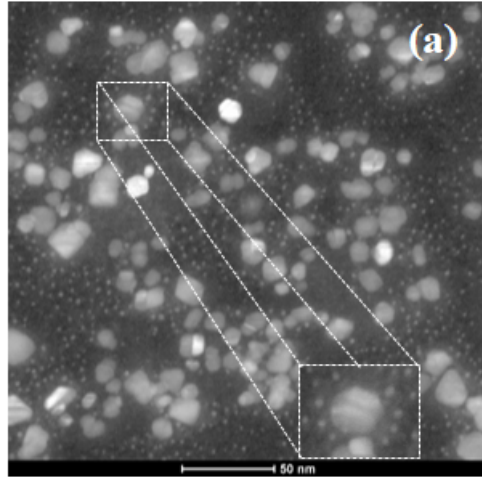
Biofilms	Carbohydrates (mg/ml)					
	NC	IONPs	CS	MCZ	IONPs-CS-MCZ31.2	IONPs-CS-MCZ78
Presence of an external magnetic field						
<i>C. albicans ATCC 10231</i>	0.74 (0.24)	0.57 (0.13)	0.56 (0.07)	0.75 (0.46)	0.74 (0.09)	0.63 (0.14)
<i>C. glabrata ATCC 90030</i>	0.47 (0.40)	1.09 (0.66)	1.16 (0.78)	0.42 (0.35)	0.82 (0.24)	0.59 (0.59)
<i>Dual-species biofilm</i>	0.77 (0.26)	0.65 (0.11)	0.62 (0.19)	0.74 (0.27)	0.74 (0.04)	0.65 (0.21)
Absence of an external magnetic field						
<i>C. albicans ATCC 10231</i>	0.68 (0.26)	0.48 (0.17)	0.62 (0.42)	0.33 (0.09)	0.53 (0.15)	0.38 (0.31)
<i>C. glabrata ATCC 90030</i>	0.81 (0.76)	1.15 (0.97)	1.50 (0.72)	0.80 (0.48)	0.80 (0.20)	0.85 (0.40)
<i>Dual-species biofilm</i>	0.55 (0.37)	0.83 (0.15)	0.52 (0.21)	0.67 (0.03)	0.84 (0.55)	0.48 (0.25)

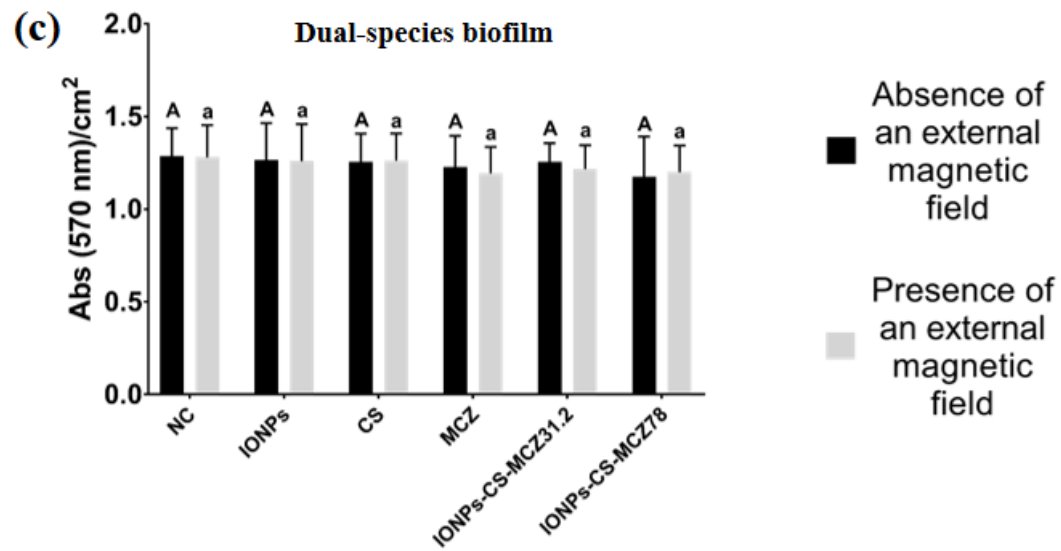
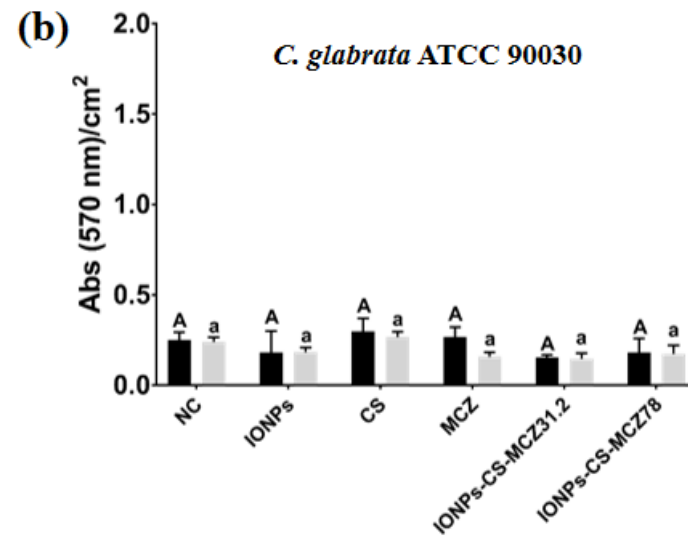
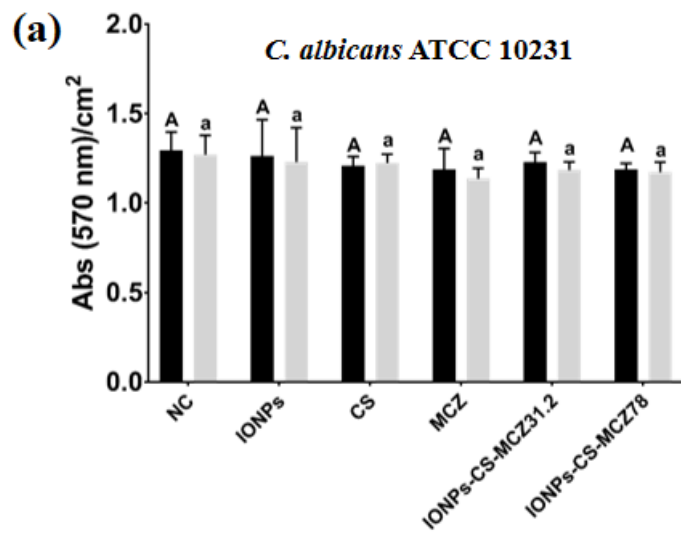
Note: there were no statistically significant differences among the compounds, regardless of the presence of a magnetic field (2-way ANOVA; $p < 0.05$). Negative control (NC); 110 $\mu\text{g/ml}$ iron oxide magnetic nanoparticles (IONPs); 110 $\mu\text{g/ml}$ chitosan (CS); 78 $\mu\text{g/ml}$ miconazole (MCZ); MCZ-containing nanocarrier at 31.2 (IONPs-CS-MCZ31.2) and 78 $\mu\text{g/ml}$ (IONPs-CS-MCZ78).

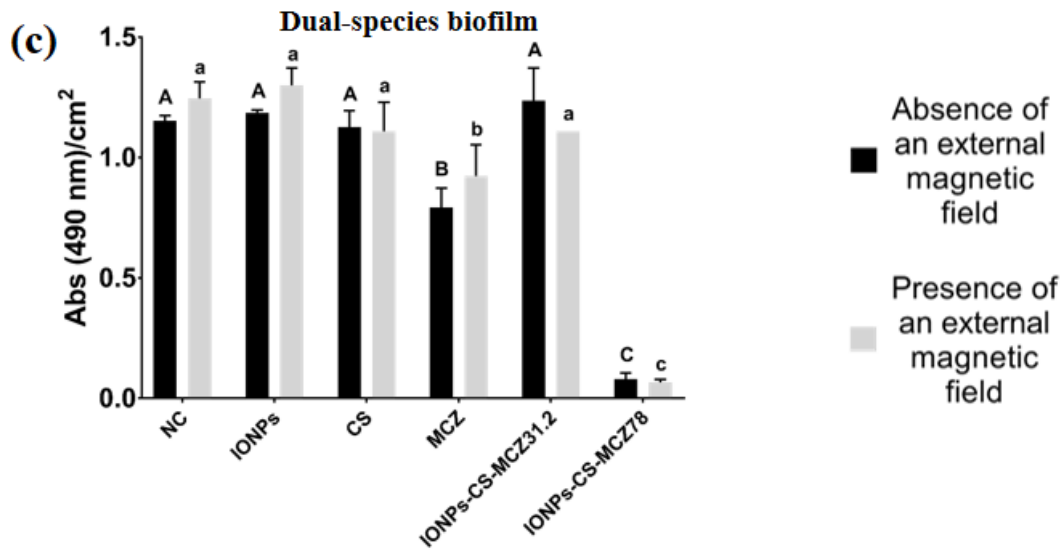
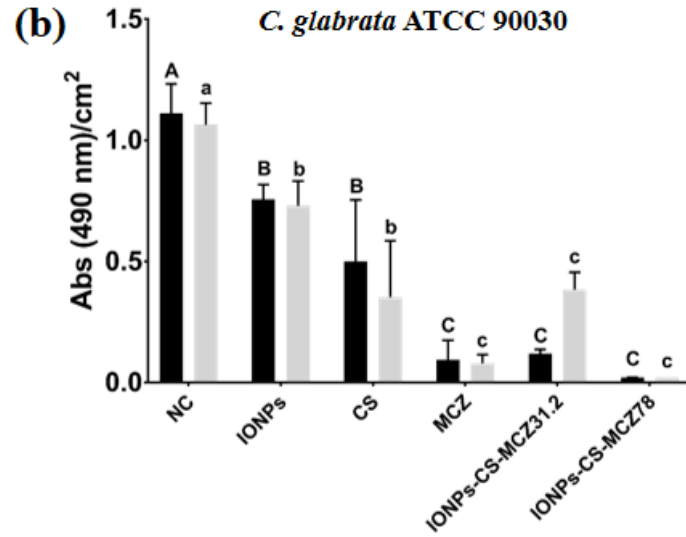
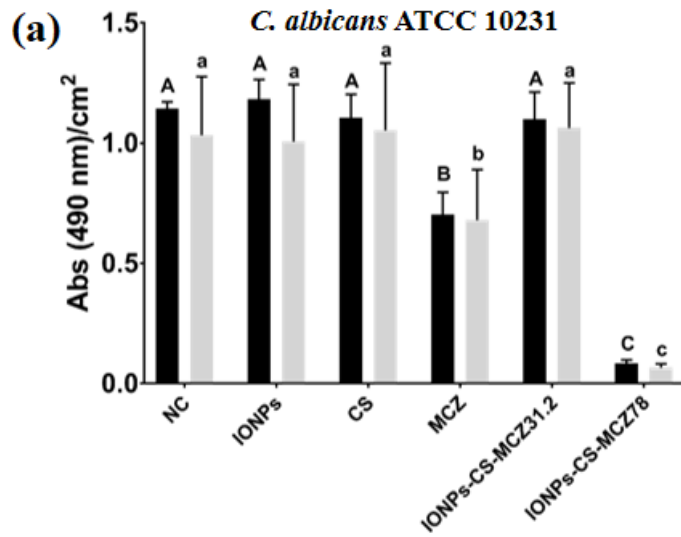
Table 4. Mean values (standard deviation) of the DNA content obtained from the extracellular matrix of single- and dual-species *Candida* biofilms after treatment with different compounds

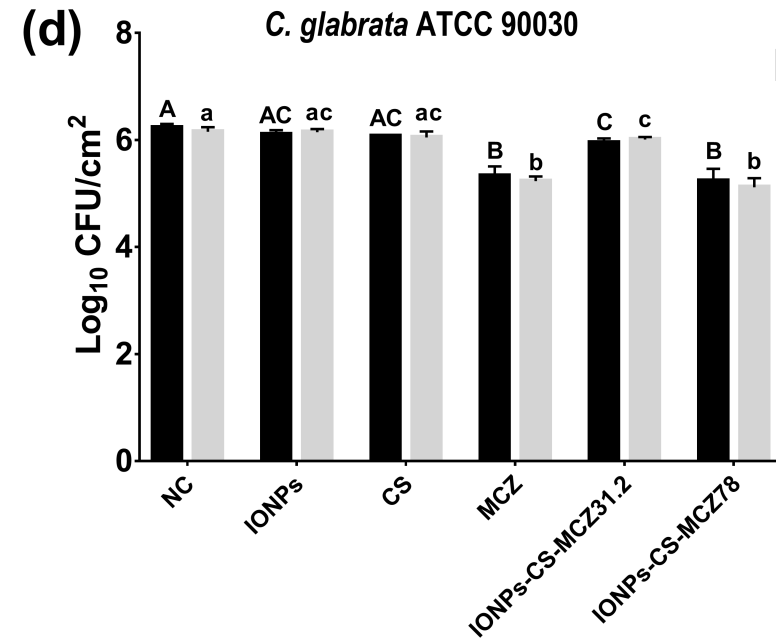
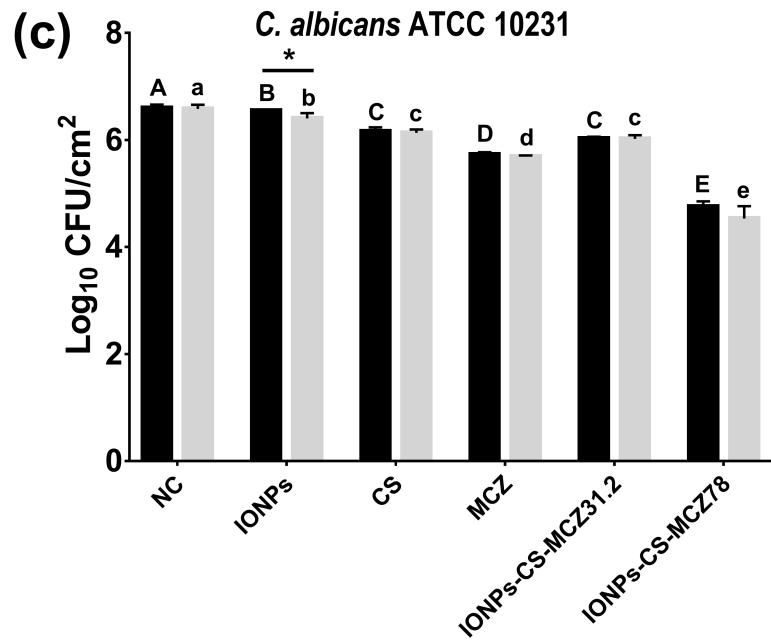
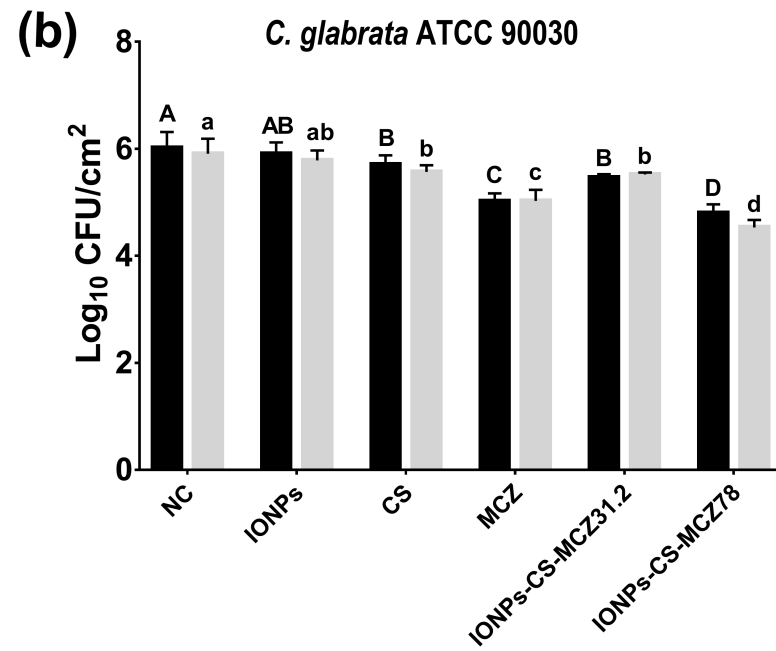
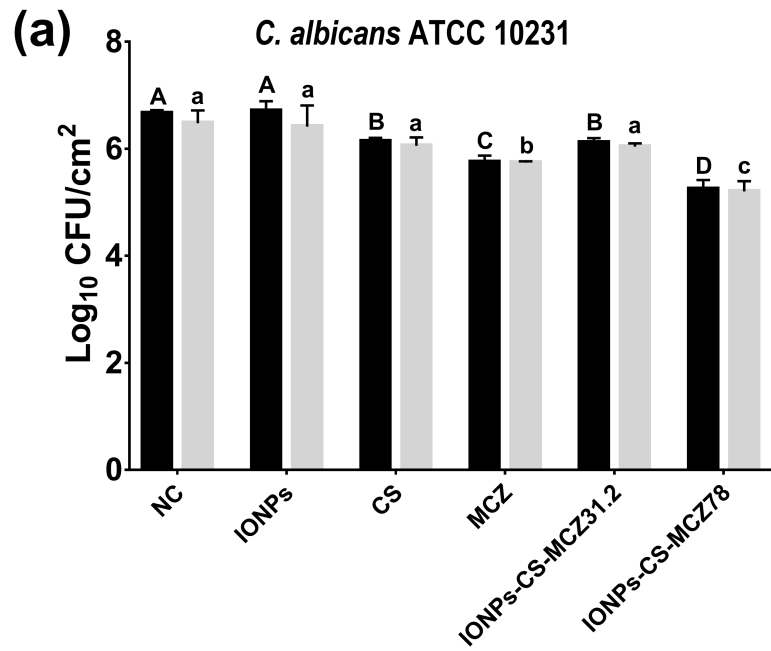
Biofilms	DNA (mg/ml)					
	NC	IONPs	CS	MCZ	IONPs-CS-MCZ31.2	IONPs-CS-MCZ78
Presence of an external magnetic field						
<i>C. albicans ATCC 10231</i>	0.03 (0.02)	0.03 (0.00)	0.02 (0.00)	0.04 (0.02)	0.04 (0.01)	0.04 (0.01)
<i>C. glabrata ATCC 90030</i>	0.01 (0.01)	0.03 (0.01)	0.03 (0.00)	0.02 (0.00)	0.02 (0.00)	0.04 (0.02)
<i>Dual-species biofilm</i>	0.04 (0.04)	0.03 (0.01)	0.03 (0.00)	0.04 (0.01)	0.04 (0.01)	0.04 (0.01)
Absence of an external magnetic field						
<i>C. albicans ATCC 10231</i>	0.03 (0.01)	0.03 (0.01)	0.02 (0.01)	0.03 (0.01)	0.04 (0.00)	0.03 (0.01)
<i>C. glabrata ATCC 90030</i>	0.02 (0.01)	0.04 (0.03)	0.04 (0.02)	0.02 (0.00)	0.03 (0.02)	0.02 (0.00)
<i>Dual-species biofilm</i>	0.03 (0.01)	0.03 (0.01)	0.03 (0.00)	0.03 (0.00)	0.04 (0.01)	0.03 (0.01)



Note: there were no statistically significant differences among the compounds, regardless of the presence of a magnetic field (2-way ANOVA; $p < 0.05$). Negative control (NC); 110 $\mu\text{g/ml}$ iron oxide magnetic nanoparticles (IONPs); 110 $\mu\text{g/ml}$ chitosan (CS); 78 $\mu\text{g/ml}$ miconazole (MCZ); MCZ-containing nanocarrier at 31.2 (IONPs-CS-MCZ31.2) and 78 $\mu\text{g/ml}$ (IONPs-CS-MCZ78).









 Absence of an external magnetic field
 Presence of an external magnetic field

